Journal of Materials Chemistry A

Overcoming Morphological and Efficiency Limit in All-Polymer Solar Cells by Designing Conjugated Random Copolymers Containing Naphtho[1,2-c:5,6-c']bis([1,2,5]thiadiazole)] Moiety

Journal:	*Journal of Materials Chemistry A*
Manuscript ID	TA-COM-09-2018-009356.R1
Article Type:	Communication
Date Submitted by the Author:	02-Nov-2018
Complete List of Authors:	Xie, Ruihao; South China University of Technology, Li, Zhenye; South China University of Technology Zhong, Wenkai; South China University of Technology, Ying, Lei; South China University of Technology, Hu, Qin; Peking University, School of Physics Liu, Feng; Shanghai Jiao Tong University Li, Ning; Friedrich-Alexander University Erlangen and Nuremberg, Institute Materials for Electronics and Energy Technology, Russell, Thomas; University of Massachusetts, Polymer Science and Engineering Department Huang, Fei; Institute of Polymer Optoelectronic Materials & Devices, Cao, Yong; Sounth China University of Technology

Journal Name

COMMUNICATION

Overcoming Morphological and Efficiency Limit in All-Polymer Solar Cells by Designing Conjugated Random Copolymers Containing Naphtho[1,2-*c*:5,6-*c*']bis([1,2,5]thiadiazole)] Moiety

Received 00th January 20xx,
Accepted 00th January 20xx

DOI: 10.1039/x0xx00000x

www.rsc.org/

Ruihao Xie‡[a], Zhenye Li‡[a], Wenkai Zhong‡[a], Lei Ying*[a], Qin Hu[c,d], Feng Liu*[b], Ning Li[e], Thomas P. Russell[c,d], Fei Huang*[a], and Yong Cao[a]

The ternary concept based on two electron donors and one electron acceptor is deployed to extend the absorption as well as photovoltaic performance of all-polymer solar cells (all-PSCs). However, it remains challenging to achieve delicate morphology of ternary blended bulk-heterojunction films through rational molecular design. To overcome these issues, here we designed and synthesized a series of narrow bandgap conjugated copolymers by combining two conjugated polymers with various molar ratios of naphthobis[1,2,5]thiadiazole (NT) unit (namely NT00-NT100). All-PSCs were constructed by integrating these resultant copolymers with a commercially available electron-accepting copolymer N2200. The resultant all-PSCs based on the ternary copolymers NT40 exihibited an impressively high power conversion efficiency over 8.0%, which obviously outperformed those of obtained from devices based on the NT00:NT100:N2200 blended films. Further characterization of the morphology of the films revealed that the incorporation of the NT unit can improve π-π stacking and a degree of phase separation conducive to exciton diffusion and charge transport.

Polymer solar cells (PSCs) have attracted much attention, since they are light-weight, show great potential for the fabrication of flexible devices based on roll-to-roll processing, and have a short energy payback time.[1-7] Considerable progress has recently been made in the development of high-performance PSCs, due to the emergence of non-fullerene acceptors (NFAs), which have high absorption coefficients that facilitate the harvesting of solar photons. [8-11] Even though all-polymer solar cells (all-PSCs) with a polymer donor and a polymer acceptor have lower photovoltaic performances than the devices based on fullerene derivatives or NFAs, they have attracted particular interest, due to their high photochemical, thermal, and mechanical stability.[12-24]

To improve the photovoltaic performance of all-PSCs, one of the critical challenges is to develop novel p-type copolymers with appropriate frontier molecular orbital energy levels and high absorption profiles that can pair with the relevant n-type copolymers.[25-27] A representative case is the recently developed electron-donating conjugated polymer comprising of an imide-functionalized benzotriazole unit in combination with an electron-accepting copolymer poly{[*N*,*N*'-bis(2-octyldodecyl)naphthalene-1,4,5,8-bis(dicarboximide)-2,6-diyl]-*alt*-5,5'-(2,2'-bithiophene)}, termed N2200, with impressively high power conversion efficiencies (PCEs) of >9%. The improved photovoltaic performance can also benefit from complementary absorption by physically blending two electron-donating polymers with an electron-accepting polymers, leading PCEs >10%.[28] However, such a ternary blending approach remains challenging, since the crystallinity, domain sizes, and domain purity are more difficult to control than with binary mixtures.[29-31]

Herein, we developed a series of ternary conjugated copolymers consisting of two electron-rich units of thiophene and benzodithiophene and an electron-deficient unit of naphtho[1,2-*c*:5,6-*c*']bis([1,2,5]thiadiazole) (NT)[32,33]. The resultant copolymers having different molar ratios of the NT moiety (10 to 100%) were synthesized by the Stille method (**Scheme S1**, in the ESI) and were named as NT10 to NT100. For comparison, the binary copolymer with alternating thiophene and benzodithiophene backbone (namely NT00) was also synthesized (**Fig. 1a**).

[a] *Institute of Polymer Optoelectronic Materials and Devices, State Key Laboratory of Luminescent Materials and Devices, South China University of Technology, Guangzhou 510640, China. Email: msleiying@scut.edu.cn; msfhuang@scut.edu.cn*
[b] *Department of Physics and Astronomy, and Collaborative Innovation Center of IFSA (CICIFSA), Shanghai Jiao Tong University, Shanghai 200240, China. Email: fengliu82@sjtu.edu.cn*
[c] *Materials Sciences Division, Lawrence Berkeley National Laboratory, Berkeley, CA 94720, USA.*
[d] *Department of Polymer Science and Engineering, University of Massachusetts Amherst, 120 Governors Drive, Amherst, MA 01003, USA.*
[e] *Institute of Materials for Electronics and Energy Technology (i-MEET), FAU Erlangen-Nürnberg, 91058 Erlangen, Germany.*
† Electronic Supplementary Information (ESI) available: [details of any supplementary information available should be included here]. See DOI: 10.1039/x0xx00000x
‡ These authors contributed equally.

The corresponding binary copolymers, namely NT00 and NT100, show highly complementary absorption spectra, and the absorption spectra of the random ternary polymers gradually broadened, increasing the absorption from 600 to 800 nm as the concentration of NT in the copolymer increased (**Fig. 1b**). The copolymer NT40 showed panchromatic absorption from 400 to 800 nm, which is advantageous for harvesting light. The highest occupied molecular orbital (HOMO) energy levels gradually decreased from –5.22 eV for NT10 to –5.52 eV for NT100, and the lowest unoccupied molecular orbital (LUMO) levels gradually decreased from –3.00 eV for NT10 to –3.40 eV for NT100 (**Fig. 1c**, **Table S1** in the ESI). The gradually decreasing HOMO energy levels with increasing NT content of these copolymers is advantageous for increasing the open-circuit voltage (V_{OC}) of all-PSCs.[34]

The photovoltaic performances of the binary and ternary all-PSCs based on the resultant polymers were evaluated in a conventional architecture of ITO/PEDOT:PSS/polymer donor:N2200/PFN-Br/Ag. Here we use poly[(9,9-bis(3'-((*N*,*N*-dimethyl)-*N*-ethylammonium)-propyl)-2,7-fluorene)-alt-2,7-(9,9-dioctylfluorene)] dibromide (PFN-Br) as the electron transport layer.[35,36] All-PSCs based on the alternative copolymers had moderate PCEs of 3.20% for NT00:N2200 (device A) and 3.51% for NT100:N2200 (device C). We then optimized the content of NT in the copolymers (**Fig. S3** and **Table S2**, ESI). The optimized all-PSC based on NT40:N2200 (device B) showed remarkable photovoltaic performance with a maximum PCE of 8.06%, with a V_{OC} of 0.80 ± 0.01 V, a short-circuit current density (J_{SC}) of 14.87 ± 0.19 mA cm^{-2}, and a fill factor (FF) of 67.16 ± 0.60%. Furthermore, we also explored the photovoltaic properties of the ternary blend all-PSCs composed of NT00:NT100:N2200 with varying weight ratios of NT100 (0-100% in 10% increments) under the same processing condition (**Fig. S4**, ESI). However, the incorporation of 40 wt% NT100 into the NT00:N2200 film (device D) only led to a PCE of 4.81%, indicating that random copolymer with panchromatic absorption can effectively improve the J_{SC} value and may yield a favorable film morphology for efficient charge transport simultaneously. It is also noteworthy that the NT40 copolymer with different molecular weight had similar PCE of ~7.9% (**Fig. S5**, ESI). The external quantum efficiency (EQE) spectra of these devices (**Fig. 2b**) agree with the corresponding absorption spectra of the blend films (**Fig. S1** in the ESI).

Photoluminescence (PL) measurements were performed to elucidate the charge generation and recombination kinetics of these all-PSCs. The PL quenching efficiency was 87.7% for device A, 97.5% for device B, 88.3% for device C and 92.6% for device D (**Fig. S6**, ESI). The highest PL quenching efficiency of 97.5% for device B indicates efficient charge carrier dissociation and improved miscibility of the copolymers and N2200. In order to investigate exciton dissociation and carrier generation, we measured the dependence of photocurrent density (J_{ph}) on the effective voltage (V_{eff}) of the devices. The photocurrent density (J_{ph}) is defined as $J_{ph} = J_L - J_D$, where J_L and J_D represent the current densities measured under illumination and in the dark, respectively. The V_{eff} is defined as $V_{eff} = V_{bi} - V_{appl}$, where V_{bi} is the voltage when $J = 0$ (the built-in voltage), and V_{appl} is the applied voltage. The exciton dissociation probability $P(E, T)$ values can be calculated from the value of the photocurrent density (J_{ph}) divided by the saturated photocurrent density (J_{sat}). The dependence of photocurrent density (J_{ph}) on the effective voltage (V_{eff}) shows that device B had the highest G_{max} and $P(E, T)$ values (**Fig. 3a** and **Table S5**, ESI),[37] indicating that device B had good exciton dissociation and carrier generation characteristics and, thus, high J_{SC} values. The charge carrier mobility was measured by space-charge-limited current (SCLC) method in hole-only and electron-only devices (**Fig. S7** and **Table S6**, ESI). All devices had similar electron-mobility (μ_e) values exceeding 1×10^{-4} cm^2 V^{-1} s^{-1}, owing to the same electron acceptor N2200 in the active layer blend films. Device B had the highest hole-mobility (μ_h) of 6.67×10^{-4} cm^2 V^{-1} s^{-1}, due to a more balanced μ_h/μ_e ratio than that for device D, which can maximize photocurrent and suppress bimolecular recombination in device B.

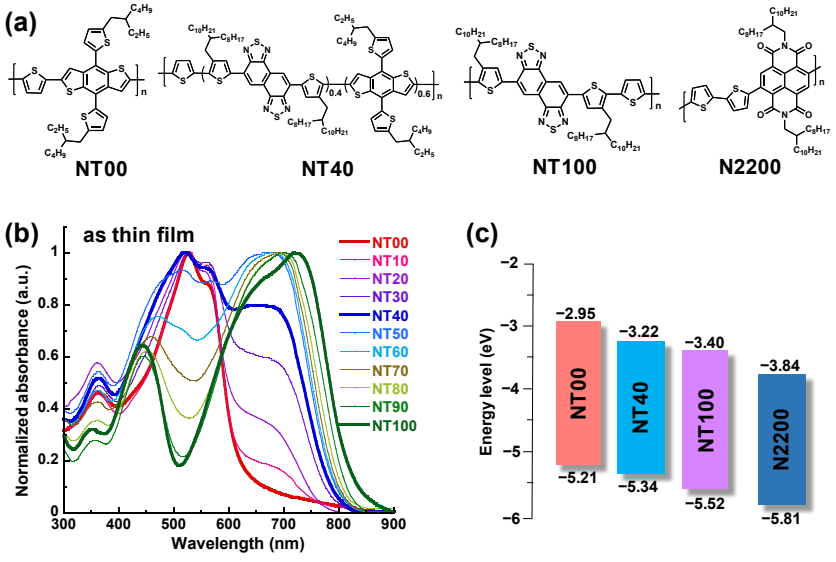

Fig. 1 (a) Molecular structures of copolymers NT00, NT40, NT100, and N2200; (b) normalized absorption spectra of NT-copolymers as thin films; (c) energy level diagram of copolymers.

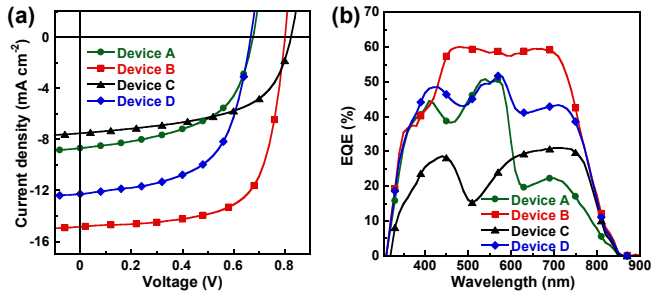

Fig. 2 (a) *J-V* characteristics and (b) EQE spectra of all-PSCs based on NT00:N2200 (2:1, wt:wt, device A), NT40:N2200 (2:1, wt:wt, device B), NT100:N2200 (2:1, wt:wt, device C) and NT00:NT100:N2200 (1.2:0.8:1, wt:wt:wt, device D).

We also measured photovoltaic parameters as a function of light intensity (P_{light}) to probe charge recombination dynamics in the photoactive layer (**Fig. 3b** and **c**). The plots of log J_{SC} versus log P_{light} are illustrated according to the power law dependence of J_{SC} upon illumination intensity, $J_{SC} \propto (P_{light})^S$, where P_{light} is light intensity and S is the exponential factor that is close to unity under weak bimolecular recombination[38]. Here, the devices A-D had very close S value approaching 1.0, showing the similar weak bimolecular recombination for these devices. The slope of V_{OC} versus the natural logarithm of P_{light} can also be used to elucidate the charge recombination mechanisms in these devices. A slope close to kT/q indicates that the bimolecular recombination is predominate and the trap-assisted mechanism is weak, where the parameters of k, T, and q represent the Boltzmann constant, temperature in Kelvin, and elementary charge, respectively[39]. As extracted from Fig. 3c, device A, B, C, and D have a slope of 1.42, 1.20, 2.13 and 1.59 kT/q, respectively. The lowest slope of device B close to kT/q

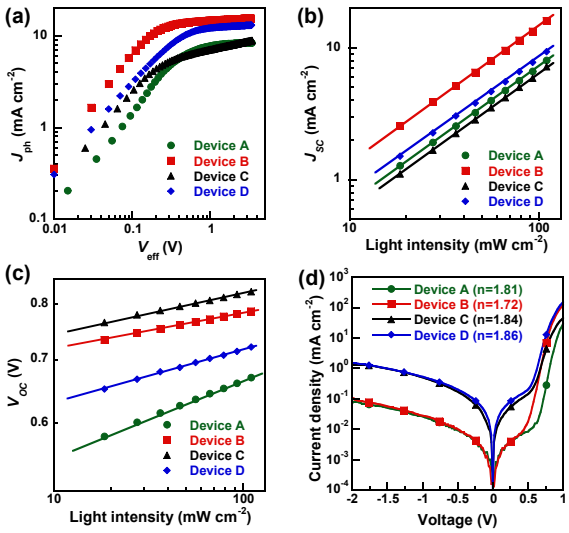

Fig. 3 (a) J_{ph}–V_{eff} curves; (b) J_{SC} and (c) V_{OC} versus light intensity (P_{light}) characteristics; (d) dark *J–V* curves and corresponding ideality factors (fitted by a one-diode equivalent circuit) for devices based on NT00:N2200 (2:1, wt:wt, device A), NT40:N2200 (2:1, wt:wt, device B), NT100:N2200 (2:1, wt:wt, device C) and NT00:NT100:N2200 (1.2:0.8:1, wt:wt:wt, device D).

suggests the suppressed trap-assisted recombination, and thus resulting in high *FF*.[38,40] **Fig. 3d** illustrates the dark J–V curves of device A-D with active layer thickness around 100 nm. The diode ideality factor (n) was obtained by fitting the dark *J–V* curves via a one diode replacement circuit.[41] The resulted diode ideality factor was 1.81, 1.72, 1.84, and 1.86 for device A, B, C, and D, respectively. The slightly lower ideality factor of device B can be understood as weaker recombination induced by defect states.

Table 1. Photovoltaic parameters measured under AM1.5 Illumination at 100 mW cm^{-2}.

Device[a]	V_{OC} (V)	J_{SC}[b] (mA cm^{-2})	$J_{SC, EQE}$[c] (mA cm^{-2})	FF (%)	PCE_{avg}[d] (%)	PCE_{max} (%)
A	0.68±0.01	8.49±0.25	8.57	54.03±0.46	3.09±0.11	3.20
B	0.80±0.01	14.87±0.19	14.55	67.16±0.60	7.92±0.14	8.06
C	0.83±0.01	7.43±0.23	7.14	56.50±0.54	3.37±0.13	3.51
D	0.67±0.01	12.28±0.31	11.77	58.97±0.61	4.62±0.18	4.81

[a] All of the blend films are processed by CF with 0.5 vol % DIO and treated with 120 °C for 10 min; [b] Obtained from *J–V* measurements; [c] Obtained from the integration of EQE spectra; [d] The PCE values are obtained from 12 separate devices. Device structure: ITO/PEDOT:PSS/active layer/PFN-Br/Ag. The composition of photoactive layer for device A: NT00:N2200 (2:1, wt:wt), device B: NT40:N2200 (2:1, wt:wt), device C: NT100:N2200 (2:1, wt:wt) and device D: NT00:NT100:N2200 (1.2:0.8:1, wt:wt:wt).

Journal Name

COMMUNICATION

Grazing-incidence wide-angle X-ray scattering (GIWAXS) was used to characterize the ordering of the neat polymers and polymer blends. As can be seen from the diffraction patterns (**Fig. S8**), NT00 shows a predominant face-on orientation, as evidenced by the (010) π-π reflection in the out-of-plane (OOP) direction at q = 1.69 Å^{-1} (d = 3.72 Å, d = 2π/q) with a crystal coherence length (CCL) of 1.78 nm, and (100) reflection in the in-plane (IP) direction characteristic of the lamellar stacking at q = 0.30 Å^{-1}. NT100 shows a compact π-π stacking distance as a sharp (010) peak emerges at a high q value of 1.81 Å^{-1} (d = 3.47 Å) with a CCL of 3.23 nm, while a small amount of the edge-on π-π stacking signal can be seen in the 2D diffraction patterns. Higher order reflections of the lamellar peak, (100) and (200), are seen for NT100 in the OOP direction, arising from the NT moieties in the conjugated backbone. Thus, the incorporation of NT into the NT00 polymer backbone has great impact on the polymer packing in the solid-state. In comparison to NT00, NT40 shows enhanced molecular co-facial packing, as indicated by the sharper (010) peak in the OOP direction at 1.71 Å^{-1} (d = 3.67 Å) with a CCL of 2.24 nm, indicating that the NT units within the polymer backbone have improved the π-π stacking and increased the crystal size of polymers. The blend films show scattering features characteristic of each component (**Fig. 4**). As shown in Fig. 4e, NT00:N2200 blend shows a broad (010) peak in the OOP direction at ~1.73 Å^{-1}; (100) reflection in the IP direction and the reflection splits into 0.25 and 0.30 Å^{-1} peaks, arising from the lamellar stacking of N2200 and NT00, respectively; (001) peak in IP direction at 0.46 Å^{-1} associated with the backbone of N2200. It should be noted that (100) peaks in OOP direction are seen for NT00:N2200 and NT40:N2200, which are not observed for the corresponding neat films, suggesting the lamellar packing of either or both materials has been improved. Comparing the NT40:N2200 binary and NT00:NT100:N2200 ternary blends, the lamellar stacking and π-π stacking regions cannot show distinct differences due to the similar scattering features of polymers. However, by normalizing the 2.5-3.0 Å^{-1} region signals in OOP direction (**Fig. S9**, ESI), NT40:N2200 blend displays more intense π-π stacking feature than that of NT00:NT100:N2200 ternary blend, which may be one of the origins of higher SCLC mobility and *FF* of NT40 based devices.

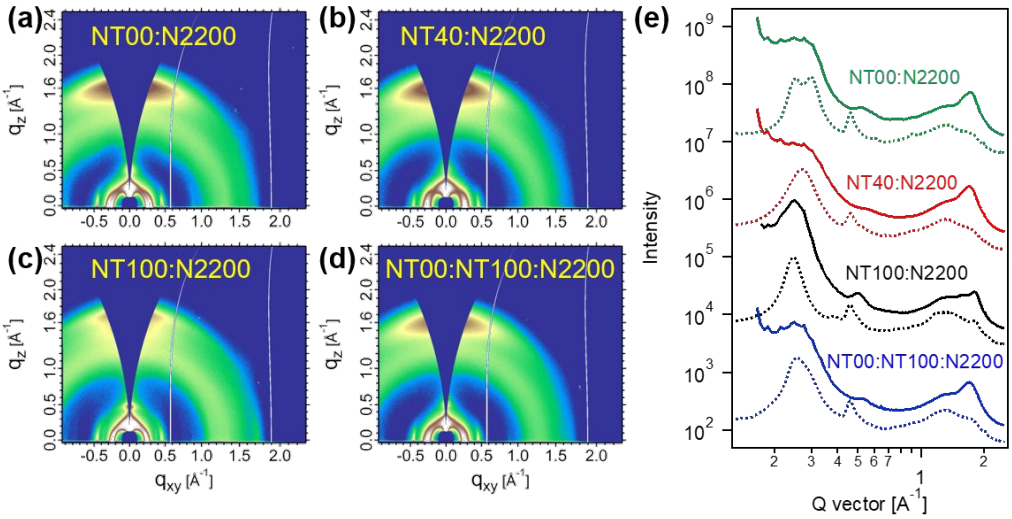

Fig. 4 (a-d) GIWAXS 2D patterns and (e) corresponding lint-cuts in OOP (solid lines) and IP (dashed lines) directions of blend films.

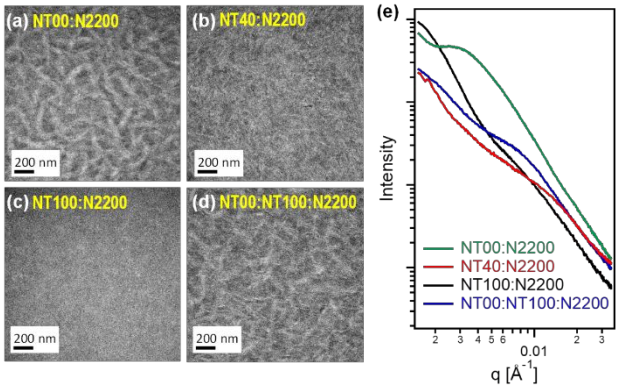

Fig. 5 (a-d) TEM images and (e) RSoXS profiles of NT00:N2200, NT40:N2200, NT100:N2200, and NT00:NT100:N2200 blend films.

The size of the phase separated domains for the all-polymer blends was characterized by transmission electron microscopy (TEM) and resonant soft X-ray scattering (RSoXS). As shown in **Fig. 5a-d**, the NT00:N2200 blend film showed large fiber-like aggregates across the entire film, while that for the NT100:N2200 blend film showed a much smaller, less well-defined texture. The NT40:N2200 blend film showed a small size scale fibrillary-like texture, while the NT00:NT100:N2200 ternary blend film showed a better-developed fibril structure, but less well-defined than the binary NT00:N2200 blend film. RSoXS profiles of the four blends using an optimized photon energy (285.2 eV) are shown in **Fig. 5e**. The NT00:N2200 blend film had an interference at q = 0.045 Å^{-1}, corresponding to a spacing of ~ 140 nm, consistent with the TEM results and the poor J_{SC} and *FF* of device A. In contrast, the scattering from the NT100:N2200 blend monotonically decreased over the entire scattering vector range with no discernable characteristic length scale. The too intimately mixed domains of NT100:N2200 are detrimental to efficient charge transport, leading to reduced J_{SC} and *FF*. This is, also, in keeping with the TEM results where phase separation, if present occurred on a very small length scale. It is reasonable to conclude that the incorporation of NT unit into conjugated polymer backbone promoted a miscibility the NT00 and N2200. This is also evident in the NT40:N2200 blend where an interference is seen at q ~ 0.016 Å^{-1}, corresponding to the average center-to-center distance of about 39 nm, much smaller than that for the NT00:N2200 and of the appropriate length scale for exciton diffusion and charge transport, and the enhanced J_{SC} and high *FF* of Device B. However, for the NT00:NT100:N2200 ternary blend film evidence for a relatively large-scale phase separation is seen with the interference occurring at q ~ 0.081 Å^{-1}, corresponding to a distance of 78 nm and in keeping with lower device performance observed. The detailed morphological characterization again underlines the significance of the findings demonstrated in this work. By combining two polymer donors in random copolymer structure with various molar ratios, the delicate bulk-heterojunction microstructural morphology can be well-controlled to facilitate efficient exciton dissociation and charge transport, which paves a way of designing novel conjugated polymers for next generation efficient all-PSCs.

In conclusion, we developed a novel concept to overcome the buk-heterojunction morphology and efficiency limit in all-PSCs by designing and synthesizing a series of ternary copolymers whose optical properties and energy levels can be effectively tuned by controlling the molar ratio of each component, enabling panchromatic absorption with suitable energy levels. All-PSCs based on the random ternary copolymer NT40 showed superior photovoltaic performance to that of its binary and ternary blended counterparts, which is attributed to its strong and broad absorption spectrum, the favourable film morphology, and suppressed recombination. Our study demonstrates that the ternary copolymers with broader absorption can open the horizon for fabricating high-performance all-PSCs; on the other hand, the desired bulk heterojunction microstructural morphology can be finely tuned by modifying the composition and molar ratio of random copolymers, leading to efficient exciton dissociation and charge transport and, as a result, enhanced photovoltaic performance. From our studies it is apparent that the photovoltaic performance of all-PSCs maybe further improved by designing efficient random copolymers with absorption covering the visible and near infrared regions.

Conflicts of interest

There are no conflicts to declare.

Acknowledgements

This work was financially supported by the National Natural Science Foundation of China (No. 21822505, 21520102006, and 51673069), and the Science and Technology Program of Guangzhou, China (No. 201710010021, 201707020019 and 2017A050503002). TPR was supported by the U.S. Office of Naval Research under contract N00014-15-1-2244. Portions of this research were conducted at beamline 7.3.3 and 11.0.1.2 at the Advanced Light Source, Molecular Foundry, Lawrence Berkeley National Laboratory, which was supported by the

Office of Science, Office of Basic Energy Sciences, of the U.S. Department of Energy under Contract No. DE-AC02-05CH11231.

Notes and references

1 J. Zhao, Y. Li, G. Yang, K. Jiang, H. Lin, H. Ade, W. Ma and H. Yan, *Nat. Energy,* 2016, **1**, 15027.

2 T. Kumari, M. L. Sang, S. H. Kang, S. Chen and C. Yang, *Energy Environ. Sci.,* 2016, **10**, 258-265.

3 S. Holliday, Y. L. Li and C. K. Luscombe, *Prog. Polym. Sci.*, 2017, **70**, 34-51.

4 K. A. Mazzio and C. K. Luscombe, *Chem. Soc. Rev.*, 2015, **44**, 78-90.

5 D. Deng, Y. Zhang, J. Zhang, Z. Wang, L. Zhu, J. Fang, B. Xia, Z. Wang, K. Lu and W. Ma, *Nat. Commun.,* 2016, **7**, 13740.

6 W. Xu and F. Gao, *Mater. Horiz.*, 2018, **5**, 206-221.

7 B. Fan, X. Du, F. Liu, W. Zhong, L. Ying, R. Xie, X. Tang, K. An, J. Xin, N. Li, W. Ma, C. J. Brabec, F. Huang and Y. Cao, *Nat. Energy*, 2018, **3**, DOI: 10.1038/s41560-018-0263-4.

8 S. Zhang, Y. Qin, J. Zhu and J. Hou, *Adv. Mater.,* 2018, **30**, 1800868.

9 P. Cheng, G. Li, X. Zhan and Y. Yang, *Nat. Photonics,* 2018, **12**, 131-142.

10 C. B. Nielsen, S. Holliday, H. Y. Chen, S. J. Cryer and I. Mcculloch, *Acc. Chem. Res.,* 2015, **48**, 2803-2812.

11 H. Bin, J. Yao, Y. Yang, I. Angunawela, C. Sun, L. Gao, L. Ye, B. Qiu, L. Xue, C. Zhu, C. Yang, Z. G. Zhang, H. Ade and Y. Li, *Adv. Mater.,* 2018, **30**, 1706361.

12 B. Fan, L. Ying, P. Zhu, F. Pan, F. Liu, J. Chen, F. Huang and Y. Cao, *Adv. Mater.,* 2017, **29**, 1703906.

13 X. Xu, Z. Li, W. Zhang, X. Meng, X. Zou, D. Di Carlo Rasi, W. Ma, A. Yartsev, M. R. Andersson, R. A. J. Janssen and E. Wang, *Adv. Energy Mater.,* 2017, **7**, 1700908.

14 Y. Zhou, T. Kurosawa, W. Ma, Y. Guo, L. Fang, K. Vandewal, Y. Diao, C. Wang, Q. Yan, J. Reinspach, J. Mei, A. L. Appleton, G. I. Koleilat, Y. Gao, S. C. B. Mannsfeld, A. Salleo, H. Ade, D. Zhao and Z. Bao, *Adv. Mater.,* 2014, **26**, 3767-3772.

15 Y. Guo, Y. Li, O. Awartani, H. Han, J. Zhao, H. Ade, H. Yan and D. Zhao, *Adv. Mater.,* 2017, **29**, 1700309.

16 S. Liu, Z. Kan, S. Thomas, F. Cruciani, J.-L. Bredas and P. M. Beaujuge, *Angew. Chem. Int. Ed.,* 2016, **55**, 12996-13000.

17 T. Kim, J.-H. Kim, T. E. Kang, C. Lee, H. Kang, M. Shin, C. Wang, B. Ma, U. Jeong, T.-S. Kim and B. J. Kim, *Nat. Commun.,* 2015, **6**, 8547.

18 T. Earmme, Y-J. Hwang, S. Subramaniyan and S.A. Jenekhe, *Adv. Mater.*, 2014, **26**, 6080-6085.

19 L. Gao, Z.-G. Zhang, L. Xue, J. Min, J. Zhang, Z. Wei and Y. Li, *Adv. Mater.,* 2016, **28**, 1884-1890.

20 B. Fan, L. Ying, Z. Wang, B. He, X.-F. Jiang, F. Huang and Y. Cao, *Energy Environ. Sci.,* 2017, **10**, 1243-1251.

21 C. Mu, P. Liu, W. Ma, K. Jiang, J. Zhao, K. Zhang, Z. Chen, Z. Wei, Y. Yi, J. Wang, S. Yang, F. Huang, A. Facchetti, H. Ade and H. Yan, *Adv. Mater.,* 2014, **26**, 7224-7230.

22 Z. Li, X. Xu, W. Zhang, X. Meng, Z. Genene, W. Ma, W. Mammo, A. Yartsev, M. R. Andersson, R. A. J. Janssen and E. Wang, *Energy Environ. Sci.,* 2017, **10**, 2212-2221.

23 D. Chen, J. Yao, L. Chen, J. P. Yin, R. Z. Lv, B. Huang, S. Q. Liu, Z. G. Zhang, C. H. Yang, Y. W. Chen and Y. F. Li, *Angew. Chem. Int. Ed.*, 2018, **57**, 4580-4584.

24 L. W. Xue, Y. K. Yang, Z. G. Zhang, X. N. Dong, L. Gao, H. J. Bin, J. Zhang, Y. X. Yang and Y. F. Li, *J. Mater. Chem. A*, 2016, **4**, 5810-5816.

25 S B. M. Savoie, S. Dunaisky, T. J. Marks and M. A. Ratner, *Adv. Energy Mater.,* 2015, **5**, 1400891.

26 H. Fu, Z. Wang and Y. Sun, *Solar RRL,* 2017, **1**, 1700158.

27 H. Li, K. Lu and Z. Wei, *Adv. Energy Mater.,* 2017, **7**, 1602540.

28 S. W. Kim, J. Choi, B. Thi Thu Trang, C. Lee, C. Cho, K. Na, J. Jung, C. E. Song, B. Ma, J.-Y. Lee, W. S. Shin and B. J. Kim, *Adv. Funct. Mater.,* 2017, **27**, 1703070.

29 I. Shin, H. j. Ahn, J. H. Yun, J. W. Jo, S. Park, S.-y. Joe, J. Bang and H. J. Son, *Adv. Energy Mater.,* 2017, **7**, 1701405.

30 J. W. Jung, F. Liu, T. P. Russell and W. H. Jo, *Energy Environ. Sci.,* 2013, **6**, 3301-3307.

31 W. Sun, Z. Ma, D. Dang, W. Zhu, M. R. Andersson, F. Zhang and E. Wang, *J. Mater. Chem. A,* 2013, **1**, 11141-11144.

32 Z. Li, L. Ying, R. Xie, P. Zhu, N. Li, W. Zhong, F. Huang and Y. Cao, *Nano Energy*, 2018, **51**, 434-441.

33 W. K. Zhong, R. H. Xie, L. Ying, F. Huang and Y. Cao, *Acta Polym. Sinica*, 2018, 217-222.

34 A. Tournebize, A. Rivaton, H. Peisert and T. Chassé, *J. Phys. Chem. C,* 2015, **119**, 9142-9148.

35 K. Zhang, F. Huang and Y. Cao, *Acta Polym. Sin.,* 2017, 1400-1414.

36 T. Jia, N. Zheng, W. Cai, L. Ying and F. Huang, *Acta Chim. Sinica,* 2017, **75**, 808-818.

37 Y. Yang, Z-G. Zhang, H. Bin, S. Chen, L. Gao, L. Xue, C. Yang, Y. Li, *J. Am. Chem. Soc.,* 2016, **138**, 15011-15018.

38 A. K. K. Kyaw, H. W. Dong, D. Wynands, Z. Jie, T. Q. Nguyen, G. C. Bazan and A. J. Heeger, *Nano Lett.,* 2013, **13**, 3796-3801.

39 Z. Li, J. Lin, H. Phan, A. Sharenko, C. M. Proctor, P. Zalar, Z. Chen, A. Facchetti, T. Q. Nguyen, *Adv. Funct. Mater.,* 2014, **24**, 6989-6998.

40 N. Gasparini, X. Jiao, T. Heumueller, D. Baran, G. J. Matt, S. Fladischer, E. Spiecker, H. Ade, C. J. Brabec, T. Ameri, *Nat. Energy*, 2016, **1**, 16118.

41 C. Waldauf, M. C. Scharber, P. Schilinsky, J. A. Hauch, C. J. Brabec, *J. Appl. Phys.,* 2006, **99**, 104503-104506.